

Searching spin-mass interaction using a diamagnetic levitated magnetic resonance force sensor

Fang Xiong,¹ Tong Wu,¹ Yingchun Leng,¹ Rui Li,^{2,3,4} Chang-Kui Duan,^{2,3,4}

Xi Kong,^{1,*} Pu Huang,^{1,†} Zhengwei Li,⁵ Yu Gao,⁵ Xing Rong,^{2,3,4} and Jiangfeng Du^{2,3,4,‡}

¹*National Laboratory of Solid State Microstructures and Department of Physics, Nanjing University, Nanjing 210093, China*

²*Hefei National Laboratory for Physical Sciences at the Microscale and Department of Modern Physics, University of Science and Technology of China, Hefei 230026, China*

³*CAS Key Laboratory of Microscale Magnetic Resonance,*

University of Science and Technology of China, Hefei 230026, China

⁴*Synergetic Innovation Center of Quantum Information and Quantum Physics, University of Science and Technology of China, Hefei 230026, China*

⁵*Key Laboratory of Particle Astrophysics, Institute of High Energy Physics, Chinese Academy of Sciences, Beijing 100049, China*

Axion-like particles (ALPs) are predicted to mediate exotic interactions between spin and mass. We propose an ALP-searching experiment based on the levitated micro-mechanical oscillator, which is one of the most sensitive sensors for spin-mass forces at a short distance. The experiment tests the spin-mass resonant interaction between the polarized electron spins and a diamagnetically levitated microsphere. By periodically flipping the electron spins, the contamination from non-resonant background forces can be eliminated. The levitated micro-oscillator can prospectively enhance the sensitivity by $10^4 \sim 10^7$ times over current experiments for ALPs with mass in the range 10 meV to 1 eV.

I. INTRODUCTION

Light pseudoscalars exist in a number of Beyond the Standard Model theories. One well-motivated example is the axion [1, 2], which is introduced via spontaneously broken the Peccei-Quinn (PQ) $U(1)$ symmetry [3, 4] to solve the strong CP problem, and also a low-mass candidate for the dark matter in the universe [5]. Generalized axion-like particles (ALPs) rise from dimensional compactification in string theory, which share similar interaction with electromagnetic fields, and share a similar phenomenological role with the axions [6–8]. Motivated by axion and ALP’s potential role in particle physics and cosmology, a number of experimental methods and techniques have been developed over the past few decades, such as the method proposed by Moody and Wilczek to detect cosmic axion [9], the photon-axion-photon conversion light shining through wall experiments [10, 11], the axion emission from the Sun [12, 13], the dichroism and birefringence effects in external fields [14, 15], and the light pseudoscalar mediated macroscopic mass-mass [16], spin-mass [17–23] and spin-spin [24, 25] forces.

The pseudoscalar exchange between fermions results in spin-dependent forces [26]. Most prior works detecting exotic spin-dependent forces [19–22, 27, 28] are focused on the so-called axion window [29], where the interaction range is $200 \mu\text{m} - 20 \text{ cm}$. Due to the interest in non-zero mass, it is desired to find experimental techniques to search for such anomalous spin-dependent interactions at even shorter distances [30].

The levitated micro-mechanical and nano-mechanical oscillators have been demonstrated as one of the ultra-sensitive force sensors [31–37] due to its ultra-low dissipation and small size. It is one of the ideal methods to measure short-range force [38–43] with high precision. However, in short-ranged force measurements, surface noises from the electric static force fluctuation, the Casimir force and magnetic force, limit the final sensitivity.

Here we propose a new method to investigate the spin-mass interaction using an ensemble of electron spins and a levitated diamagnetic microsphere mechanical oscillator. By periodically flip the electron spin at the resonant frequency with the mechanical oscillator, the postulated force between electron spins and the microsphere mass is preserved while the spin-independent force noise from the surface is eliminated.

II. SCHEME

We use a levitated diamagnetic microsphere mechanical oscillator to investigate the spin-mass interaction (Fig. 1(a)). The microsphere is trapped in the magneto-gravitational trap and levitated stably in high vacuum. The diamagnetic-levitated micro-mechanical oscillator achieves the best sensitivity in micro- and nano-mechanical systems to date, orders of magnitude improvement over the reported state-of-the-art systems based on different principles. The cryogenic diamagnetic-levitated oscillator described here is applicable to a wide range of mass, making it a good candidate for measuring force with ultra-high sensitivity [44]. The position of the microsphere is mainly determined by the equilibrium between the gravity force and the main magnetic force of

* kongxi@nju.edu.cn

† hp@nju.edu.cn

‡ djf@ustc.edu.cn

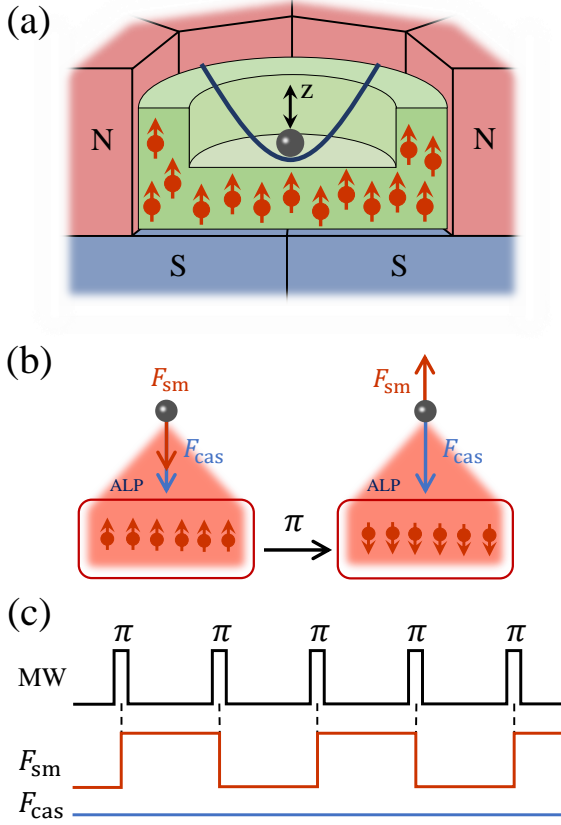


FIG. 1. (a) Schematic of the proposed experimental system. The red and blue parts of the N and S poles represent the profile of the permanent magnet, and the green part represents the profile of the spin source. We use a microsphere as the force sensor, which is placed in the magneto-gravitational trap above the surface of the spin source (see Appendix A for the description of its motion). The geometry is sophisticated designed to eliminate the spin-induced magnetic force on the levitated microsphere (see Appendix C for details). (b) Flipping of the electron-spins by a microwave π . The spin mass force F_{sm} flips with these spins, while those spin-independent forces, for example, the Casimir force F_{cas} , are independent of the spins and therefore do not flip with the spins. (c) Microwave (MW) pulse sequences. The spins flip at $2\omega_z$, twice the resonance frequency of the levitated oscillator. This leads to a periodical force F_{sm} of the frequency ω_z , while the spin-independent forces such as Casimir force F_{cas} remains constant during the measurement.

the trap. A uniform magnetic field is applied to tune the levitation position (see Appendix A). A groove-shaped electron spin ensemble (see Appendix C for detail) is located below the mass source as a spin source.

The spin-mass interaction between a polarized electron and an unpolarized nucleon is: [26]:

$$V(\hat{\sigma}, r) = \frac{\hbar^2 g_s^N g_p^e}{8\pi m_e} (\hat{\sigma} \cdot \mathbf{e}_r) \left(\frac{1}{\lambda r} + \frac{1}{r^2} \right) e^{-r/\lambda}, \quad (1)$$

where g_s^N and g_p^e are the coupling constants of the in-

teraction, with g_s^N representing the axion scalar coupling constant to an unpolarized nucleon and g_p^e representing the axion pseudoscalar coupling constant to the electron spin, $\lambda = \hbar/(m_a c)$ is the interaction range, m_a is the ALP mass, m_e is the mass of electron, $\hat{\sigma}$ is electron spin operator, r is the displacement between the electron and nucleon, and \mathbf{e}_r is the direction. The spin-mass force along z axis is calculated by integrating the force element between microsphere and spin-source based on Eq.(1) as:

$$F_{sm}(t) = \rho_e(t) \frac{\hbar^2 g_s^N g_p^e \rho_m}{8\pi m_e} \zeta_{sm}(R, d, \lambda), \quad (2)$$

where $\rho_e(t)$ is the time dependent net electron spin density along z axis, ρ_m is the nucleon density of the microsphere $\zeta_{sm}(R, d, \lambda)$ is the effective volume for spin-mass interaction that depends on geometry parameters (see Appendix D), R is the microsphere radius and d is the surface distance between the mass and the spin-source.

The electrons spins are initially polarized along the magnetic field under high field and low temperature, so that $\rho_e(0) = \rho_{e0}$, where ρ_{e0} is the electron density of the spin-source. Then they are flipped periodically in resonance with the microsphere mechanical oscillator (see Fig. 1(b)). On one hand, the spin-independent interactions, such as the Casimir force, will be off-resonance and become eliminated (Fig. 1(c)). On the other hand, the spin-mass interaction is preserved on the resonance condition. The spin autocorrelation function is defined as $\langle \rho_e(t) | \rho_e(0) \rangle = \rho_e(0)^2 P(t) = \rho_e(0)^2 e^{-t/T_1} \xi(t)$, where T_1 is the electron spin-lattice relaxation time and $\xi(t)$ is the modulation function (see Appendix B). The microwave π pulses flip the electron spin periodically with frequency $2\omega_z$. $\xi(t)$ jump between -1 and +1 every time the electron spins are flipped. The corresponding power spectral density (PSD) of the spin-related force is proportional to $\tilde{G}(\omega)$, which is the Fourier transform of $P(t)$. The PSD of spin-mass force is then :

$$S_{ff}^{sm}(\omega) = \left(\frac{\hbar^2 g_s^N g_p^e \rho_m}{8\pi m_m} \zeta_{sm}(R, d, \lambda) \right)^2 \rho_{e0}^2 \tilde{G}(\omega). \quad (3)$$

If spin-mass interaction signal is observed on resonance ($\omega = \omega_z$), the coupling $g_s^N g_p^e$ can be derived as

$$g_s^N g_p^e = \sqrt{\frac{S_{ff}^{sm}(\omega_z)}{\tilde{G}(\omega_z)}} \frac{8\pi m_e}{\zeta_{sm} \hbar^2 \rho_m \rho_{e0}}. \quad (4)$$

Apart from the spin-mass force, spin-induced magnetic force F_s between electron spins and the diamagnetic microsphere is recorded during the measurement. Fortunately, well designed spin-source geometry can eliminate most of the force (see Appendix C). Then the residual spin-induced magnetic force is

$$F_s(t) = \rho_e(t) \frac{\mu_B \chi_m}{2} \frac{\partial B_{0z}}{\partial z} \zeta_s(R, d), \quad (5)$$

where $\zeta_s(R, d)$ is the effective volume for spin-induced force. Similarly, the PSD of F_s is

$$S_{\text{ff}}^s(\omega) = \left(\frac{1}{2} \mu_B \chi_m \frac{\partial B_{0z}}{\partial z} \zeta_s(R, d) \right)^2 \rho_{e0}^2 \tilde{G}(\omega). \quad (6)$$

Considering the fluctuating noise, the equation of motion for the system center of mass is

$$m\ddot{z} + m\gamma\dot{z} + m\omega_z^2 z = F_{\text{flu}}(t) + F_s(t) + F_{\text{sm}}(t), \quad (7)$$

where m is the mass of the microsphere, $\omega_z/2\pi$ is the resonance frequency, $\gamma/2\pi$ is the intrinsic damping rate and $F_{\text{flu}}(t)$ is the fluctuating noise force that includes the thermal Langevin force $F_{\text{th}}(t)$ and the radiation pressure fluctuations $F_{\text{ba}}(t)$ [45].

The total detected displacement PSD is given by:

$$S_{zz}^{\text{tot}}(\omega) = S_{zz}^{\text{imp}}(\omega) + \frac{|\chi(\omega)|^2}{m^2} (S_{\text{ff}}^{\text{ba}} + S_{\text{ff}}^{\text{th}} + S_{\text{ff}}^s + S_{\text{ff}}^{\text{sm}}) \quad (8)$$

where $\chi(\omega)$ is the mechanical susceptibility given by $|\chi(\omega)|^2 = 1/[(\omega_z^2 - \omega^2)^2 + \gamma^2\omega^2]$; $S_{zz}^{\text{imp}}(\omega)$ denotes the PSD of the detector imprecision noise; $S_{\text{ff}}^{\text{ba}}$, $S_{\text{ff}}^{\text{th}}$, S_{ff}^s and $S_{\text{ff}}^{\text{sm}}$ are the PSDs of $F_{\text{ba}}(t)$, $F_{\text{th}}(t)$, $F_s(t)$ and $F_{\text{sm}}(t)$, respectively. The total fluctuation noise $S_{\text{ff}}^{\text{flu}}(\omega_z) = S_{\text{ff}}^{\text{th}} + S_{\text{ff}}^{\text{ba}} + m^2 S_{zz}^{\text{imp}} |\chi(\omega_z)|^{-2}$. Due to these noises, the detection limit of spin-mass coupling strength $g_s^N g_p^e$ is thus:

$$(g_s^N g_p^e)_{\text{limit}} = \sqrt{\frac{S_{\text{ff}}^{\text{flu}}(\omega_z) + S_{\text{ff}}^s(\omega_z)}{\tilde{G}(\omega_z)}} \frac{8\pi m_e}{\zeta_{\text{sm}} \hbar^2 \rho_m \rho_{e0}}. \quad (9)$$

III. RESULTS

As a reasonable example we consider a microsphere with mass $m = 1.5 \times 10^{-13} \text{ kg}$ and radius $R = 3.2 \mu\text{m}$ of density $1.1 \times 10^3 \text{ kg/m}^3$. Thus, the corresponding nucleon density is $\rho_m = 6.7 \times 10^{29} \text{ m}^{-3}$. The magnetic susceptibility of the microsphere is -9.1×10^{-6} . The whole system is placed in a cryostat with temperature $T = 20 \text{ mK}$ and external uniform magnetic field $B_{\text{ext}} = 1.85 \text{ T}$. A permanent magnet provides 0.15 T magnetic field and correspondingly the z direction magnetic gradient $\partial B_{0z}/\partial z = 750 \text{ T/m}$. The microsphere is then levitated with a surface distance $d = 1.46 \mu\text{m}$ above the spin source. The whole mechanical oscillator system have a typical frequency of 24 Hz [46] and the electron density of the spin-source is $\rho_{e0} = 2.3 \times 10^{27} \text{ m}^{-3}$. The direction of the electron spins is initially prepared along the external magnetic field, which in our design is approximately along the z axis, with a maximum tilted angle of 4° .

The total measurement time is set as 1 s . We take the experimental sensitivity limited by the total fluctuation noise as $S_{\text{ff}}^{\text{flu}}(\omega_z) = S_{\text{ff}}^{\text{th}} + S_{\text{ff}}^{\text{ba}} + m^2 S_{zz}^{\text{imp}} |\chi(\omega_z)|^{-2}$. Here $S_{\text{ff}}^{\text{th}}$ is estimated to be $5.14 \times 10^{-43} \text{ N}^2/\text{Hz}$ according to $S_{\text{ff}}^{\text{th}} = 4m\gamma k_B T$, with $\gamma/2\pi = 10^{-6} \text{ Hz}$ [44].

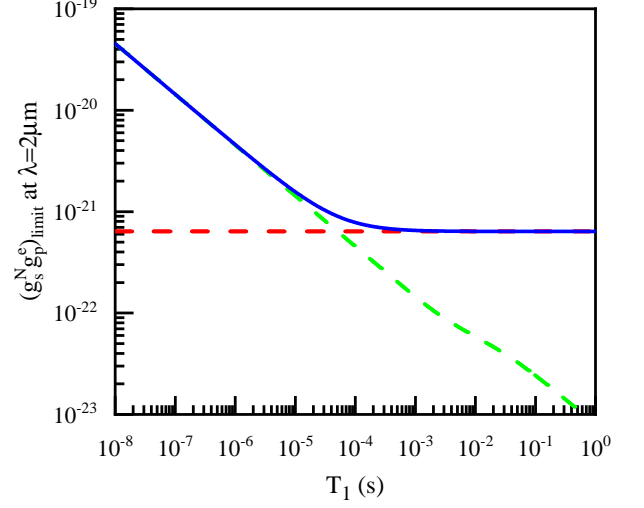


FIG. 2. $(g_s^N g_p^e)_{\text{limit}}$ for the force range of $\lambda = 2 \mu\text{m}$ as an example. The green line denotes $(g_s^N g_p^e)_{\text{limit}}$ calculated from the total fluctuation noise, which decreases as T_1 increases; the red line denotes the correction of $(g_s^N g_p^e)_{\text{limit}}$ by taking the residual spin-induced magnetic force into account, which is independent of T_1 ; the blue curve denotes their sum. The correction from spin-induced magnetic force (red curve) is dominant when $T_1 > 1 \text{ ms}$.

Imprecision noise and backaction noise are related, when they contribute equally, the sum has a minimum $S_{\text{ff}}^{\text{sum}}(\omega_z) = S_{\text{ff}}^{\text{ba}} + m^2 S_{zz}^{\text{imp}} |\chi(\omega_z)|^{-2} = 2m |\chi(\omega_z)|^{-1} \hbar / \eta^{\frac{1}{2}}$. In a practical condition, the measurement efficiency $\eta \geq 0.001$ [47], which imply $S_{\text{ff}}^{\text{sum}}(\omega_z) = 9.36 \times 10^{-49} \text{ N}^2/\text{Hz}$. Thus, the total fluctuation noise is dominated by the thermal noise, with $S_{\text{ff}}^{\text{flu}}(\omega_z) \approx 5.14 \times 10^{-43} \text{ N}^2/\text{Hz}$. Under such an experimental sensitivity, $(g_s^N g_p^e)_{\text{limit}} = 8\pi m_e (S_{\text{ff}}^{\text{flu}}(\omega_z) / \tilde{G}(\omega_z))^{\frac{1}{2}} / \zeta_{\text{sm}} \hbar^2 \rho_m \rho_{e0}$. As $\tilde{G}(\omega_z)$ is proportional to the electron spin-lattice relaxation time, $(g_s^N g_p^e)_{\text{limit}}$ decreases as T_1 increases, which is shown in green in Fig. 2.

Practically, it is not feasible to completely eliminate the spin-induced magnetic force due to fabrication imperfection of the spin-source geometry (see Appendix C). A correction for $(g_s^N g_p^e)_{\text{limit}}$ is introduced as follows. Since the spin-induced magnetic noise is spin-dependent while the $\tilde{G}(\omega_z)$ has the same scaling, its contribution to $(g_s^N g_p^e)_{\text{limit}}$ is constant (blue curve in Fig. 2). For $T_1 > 1 \text{ ms}$, the $(g_s^N g_p^e)_{\text{limit}}$ is dominated by the spin-induced magnetic force and approaches to the minimum $8\pi m_e (S_{\text{ff}}^s(\omega_z) / \tilde{G}(\omega_z))^{\frac{1}{2}} / \zeta_{\text{sm}} \hbar^2 \rho_m \rho_{e0}$.

Finally, Fig. 3 shows the calculated $(g_s^N g_p^e)_{\text{limit}}$ (see Appendix E) set by this work at $\lambda = 0.1 \mu\text{m} - 300 \mu\text{m}$ together with reported experimental results for the constraints of spin-mass coupling. Here our result is estimated through supposing $T_1 = 1 \text{ s}$, for spin-lattice relaxation time can be longer than the scale of seconds at low temperature [48, 49]. The limitation for our pro-

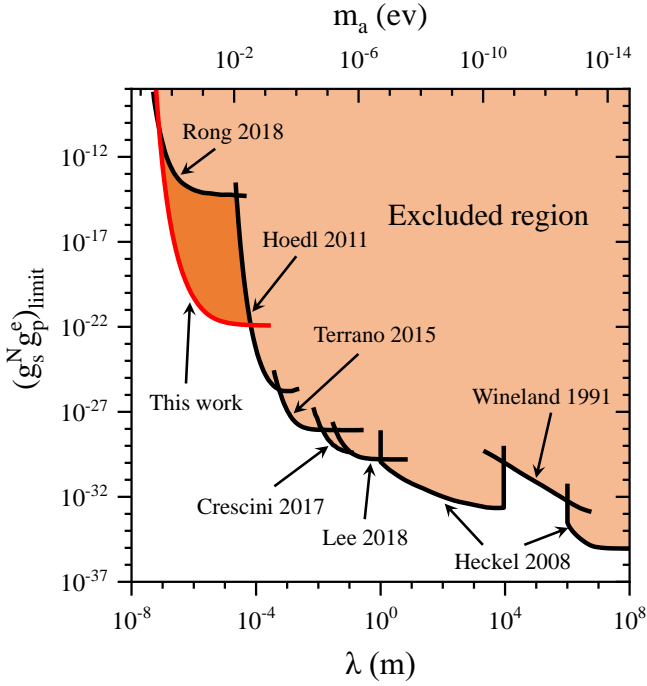


FIG. 3. $(g_s^N g_p^e)_{\text{limit}}$ as a function of the interaction range λ . Black solid lines represent the results from refs. [17, 23, 25, 50–53]. The estimated bound of our method is plotted in red for the spin-mass force range $\lambda = 0.1 \mu\text{m} - 300 \mu\text{m}$. Our result is 4 to 7 orders of magnitude more stringent in the ALP mass range of 10 meV – 1 eV compared with those from ref. [50, 51].

positional is the residual spin-induced magnetic force, which can not be eliminated by spin flip procedures. For $\lambda = 2 \mu\text{m}$, the minimum detectable spin-mass coupling is $(g_s^N g_p^e)_{\text{limit}} = 6.3 \times 10^{-22}$ (Table I) due to the spin-induced magnetic noise S_{ff}^s under reasonable fabrication imperfection $\Delta\zeta_s = 1.38 \times 10^{-21} \text{ m}^3$ (see Appendix C). In conclusion, compared to those from ref. [50, 51], our result shows an improvement of 4 to 7 orders of magnitude more stringent in the ALP mass range of 10 meV – 1 eV.

IV. DISCUSSION

The 4 to 7 orders of magnitude enhancement in our scheme comes from the following two aspects. Firstly, the magnetic resonance spin flipping is applied to suppress the short-range force noise which limits the precision of probing spin-mass coupling. Secondly, the diamagnetic levitation realizes an ultra-low dissipation in comparison with other reported mechanical systems, and this together with low temperature condition provides an ultra-low detection noise. The main limitation of our method comes from the spin-induced magnetic force that evolves in accord with the spin-mass interaction, which cannot be eliminated with finite size of the force sensor and imperfect geometric symmetry in the layout of

the electron spins. Such a magnetic background could be measured by a sensitive magnetometer with high spatial resolution, such as a single NV center, and then be subtracted from the measured signal, leading to more stringent constraints of the spin-mass coupling strength $g_s^N g_p^e$.

ACKNOWLEDGMENTS

This work was supported by the National Key R&D Program of China (Grant No. 2018YFA0306600), the National Natural Science Foundation of China (Grant No. 61635012, No. 11675163, No. 11890702, No. 12075115, No. 81788101, No. 11761131011, No. 11722544 and No. U1838104), the CAS (Grant No. QYZDY-SSW-SLH004, No. GJJSTD20170001, and No. Y95461A0U2), the Fundamental Research Funds for the Central Universities (Grant No. 021314380149), and the Anhui Initiative in Quantum Information Technologies (Grant No. AHY050000).

Appendix A: DYNAMICS OF MICRO-SPHERE OSCILLATOR

For the microsphere, the dynamics in the z direction of its center of mass (CM) in our system reads:

$$m\ddot{z} = -m\gamma\dot{z} + F_{\text{sm}} + F_s + F_{\text{flu}} + \frac{-\partial E_p}{\partial z}, \quad (\text{A1})$$

where $m\gamma\dot{z}$ is the residual air damping force, F_{sm} is spin-mass force, F_s is the spin-induced magnetic force, F_{flu} is the fluctuating noise force. E_p is the trap potential subject to gravitational field, main magnetic field, spin-induced magnetic field, and Casimir attractive force, i.e.,

$$E_p = mgz + \int_{\text{m}} dV \frac{\chi_{\text{m}}}{2\mu_0} B_{0z}^2 + \int_{\text{m}} dV \frac{\chi_{\text{m}}}{2\mu_0} B_{sz}^2 + V_{\text{cas}}, \quad (\text{A2})$$

where mgz is the gravity of microsphere, $\int_{\text{m}} dV$ represents the volume integral over the microsphere, μ_0 is permeability of vacuum, and χ_{m} is magnetic susceptibility of the microsphere. B_{0z} is the main magnetic field at the center-mass (CM) of the microsphere, which is the sum of the magnetic field generated by permanent magnet and the uniform external magnetic field B_{ext} . B_{sz} accounts for the spin-induced magnetic field, and V_{cas} is the Casimir potential [54–57] between the surface of microsphere and the surface of spin-source, reads as,

$$V_{\text{cas}} = -\frac{\hbar c \pi^2}{1440(z+d)^2} 2\pi R \eta_c, \quad (\text{A3})$$

where R is the radius of the microsphere, z corresponds to the displacement of the microsphere, $d = 1.46 \mu\text{m}$ is the surface distance between the microsphere and the

TABLE I. Contributions to the power spectral density (PSD)

PSD calculated at $T_1 = 1\text{s}$	Size (N^2/Hz)	Contribution to $(g_s^N g_p^e)_{\min}$ at $\lambda = 2\text{ }\mu\text{m}$
Of spin induced magnetic force $S_{\text{ff}}^s(\omega_z)$	2.59×10^{-41}	6.3×10^{-22}
Of thermal noise $S_{\text{ff}}^{\text{th}}(\omega_z)$	5.14×10^{-43}	9.1×10^{-24}
Of backaction noise plus imprecision noise $S_{\text{ff}}^{\text{add}}(\omega_z)$	9.36×10^{-49}	1.2×10^{-26}
Total	2.59×10^{-41}	6.3×10^{-22}

spin source when the microsphere locates in equilibrium (Fig. 4), $\eta_c = 0.059$ characterizes the reduction in the Casimir force, depending on the dielectric functions of the microsphere and the spin-source. The value of E_p versus the displacement of the microsphere is shown in Fig. 4.

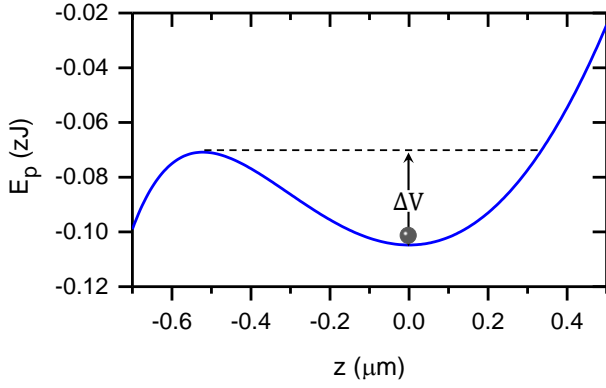


FIG. 4. The magneto-gravity potential E_p as a function of the displacement of the microsphere. The depth of the trap is $\Delta V = 3.4 \times 10^{-23} \text{ J}$. According to the energy equipartition theorem, the thermal energy at 20 mK is $1.38 \times 10^{-25} \text{ J}$, which implies that the microsphere will not escape the trap.

Thus our mechanical system can be described as a damping harmonic oscillator subject to F_{sm} , F_s and F_{flu} , i.e.,

$$m\ddot{z} + m\gamma\dot{z} + m\omega_z^2 z = F_{\text{sm}} + F_s + F_{\text{flu}}, \quad (\text{A4})$$

where ω_z is the resonant frequency of the microsphere,

$$\omega_z = \sqrt{\frac{1}{m} \frac{\partial E_p}{\partial z}}. \quad (\text{A5})$$

The equilibrium position of the microsphere can be derived by $\partial E_p / \partial z = 0$. The spin-induced magnetic field and V_{cas} are so weak that they have negligible influence on this trap, so that the equilibrium position is mainly determined by the gravity field and the main magnetic field B_{0z} . Thus we can indirectly tune it by the uniform external magnetic field B_{ext} .

Appendix B: AUTOCORRELATION FUNCTION OF NET ELECTRON-SPINS DENSITY

The autocorrelation function of electron polarization is $\langle \rho_e(t) \rho_e(0) \rangle$. Suppose these electron spins are indepen-

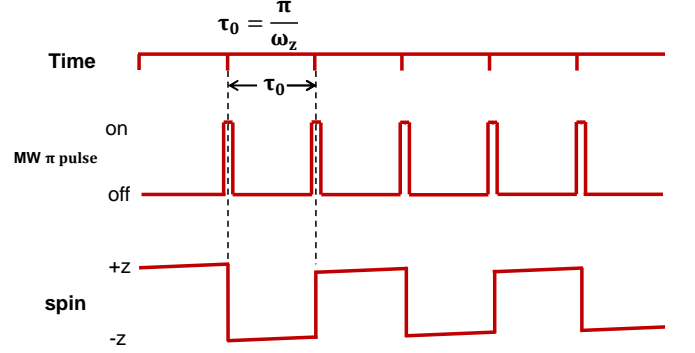


FIG. 5. Microwave π pulses carried on with a frequency of $2\omega_z$. The time interval between two adjacent π pulses is $\tau_0 = \pi/\omega_z$. Spin flips with a frequency of ω_z and its amplitude varies slowly over time due to the spin-lattice relaxation.

dent of each other, we have

$$\langle \rho_e(t) \rho_e(0) \rangle = \rho_{e0}^2 P(t), \quad (\text{B1})$$

where $P(t)$ is the autocorrelation function of a single spin, i.e.,

$$P(t) = p_{\uparrow}(t) - p_{\downarrow}(t). \quad (\text{B2})$$

Here $p_{\uparrow,\downarrow}(t)$ represents the spin population on $|\uparrow\rangle$ or $|\downarrow\rangle$. Every time when a π pulse is applied to flip the electron spin,

$$\begin{aligned} p_{\uparrow}(t) &= p_{\uparrow}(t) + p_{\downarrow}(t)p_1(\tau) \\ p_{\downarrow}(t) &= p_{\downarrow}(t)(1 - p_1(\tau)), \end{aligned} \quad (\text{B3})$$

where $\tau \in (0, \tau_0)$, τ_0 corresponds to the period between two adjacent π pulses (Fig. 5), $p_1(\tau) = 1 - e^{-\tau/T_1}$ is the spin flip probability during τ_0 , T_1 is spin-lattice relaxation time.

The evolution of $P(t)$ is shown in Fig. 6(a). $P(t)$ presents a sawtooth-like wave of frequency $2\omega_z$ for $t = k\tau_0 + \tau \gg T_1$, ($k=0, 1, 2, \dots$),

$$P(\tau + k\tau_0) = 1 - \frac{2e^{-\frac{\tau}{T_1}}}{1 + e^{-\frac{\tau_0}{T_1}}}, \quad \tau \in (0, \tau_0) \quad (\text{B4})$$

Only the signal with resonant frequency ω_z needs to be collected. After dropping the sawtooth-like signal whose frequency is $2\omega_z$, the resonant signal is shown in Fig. 6(b). The resonant signal is a square wave with an exponential decay, i.e.,

$$P(t) = e^{-t/T_1} \xi(t), \quad (\text{B5})$$

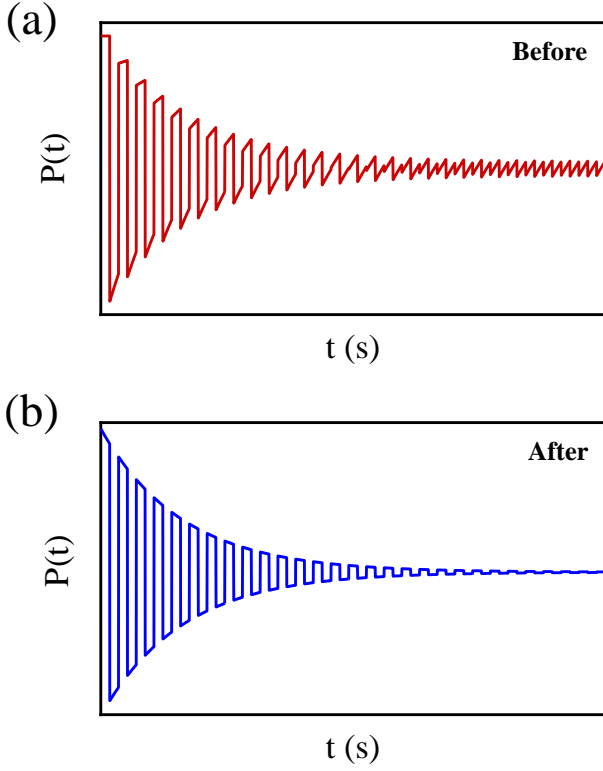


FIG. 6. (a) Variation of the native $P(t)$ after equilibrium in the form of a sawtooth-like wave. The frequency of the sawtooth-like wave is $2\omega_z$, which is out of resonance with the microsphere oscillator and can be neglected. (b) Effective $P(t)$ after dropping the sawtooth-like wave. It is a square wave modulated signal that decays exponentially with time, which is determined by the spin-lattice relaxation time. The frequency of this signal is ω_z .

where $\xi(t)$ is the modulation function of the following form

$$\xi(t) = \frac{2}{1 + e^{-\frac{\tau_0}{T_1}}} \varsigma(\omega_z t + \frac{\pi}{2}). \quad (\text{B6})$$

Here $\varsigma(\omega_z t + \frac{\pi}{2})$ is a square wave of frequency ω_z . According to the Wiener-Khinchine theorem, its single side PSD is:

$$\tilde{G}(\omega) = \frac{4}{1 + e^{-\tau_0/T_1}} \left(\frac{2T_1}{1 + T_1^2 \omega^2} - 4e^{-\tau_0/2T_1} \frac{T_1 (1 + e^{-\tau_0/T_1}) \cos(\omega\tau_0/2) - \omega (1 - e^{-\tau_0/T_1}) \sin(\omega\tau_0/2)}{(1 + T_1^2 \omega^2) (1 + e^{-2\tau_0/T_1} + 2e^{-\tau_0/T_1} \cos(\omega\tau_0))} \right).$$

Appendix C: PSD OF SPIN INDUCED MAGNETIC FORCE

Apart from the desired magnetic trap, the spin-source can induce a magnetic force F_s on the microsphere as follows

$$F_s = \int_m dV \frac{\chi_m}{\mu_0} \left(B_{0z} \frac{\partial B_{sz}}{\partial z} + B_{sz} \frac{\partial B_{0z}}{\partial z} \right).$$

This force can be eliminated by deliberately designing the configuration of spin source (in Fig. 7).

The z -direction component of magnetic field produced by a single spin is

$$B_{sz0} = \frac{\mu_0 \mu_B}{4\pi} \frac{3\cos^2\theta - 1}{l^3}, \quad (\text{C1})$$

where θ is the polar angle and l is the distance from the microsphere to the spin. The magnetic field of a spin-source cylinder at z axis is then

$$B_{sz_i} = \int_{\text{cyl}_i} dV \rho_e(r_i, z_i, t) B_{sz0}. \quad (\text{C2})$$

Here $i = 1$ and 2 correspond to cylinder1 and cylinder 2, $\int_{\text{cyl}_i} dV = \int_{-R_{si}}^{R_{si}} dz_i \int_0^{\sqrt{R_{si}^2 - z_i^2}} 2\pi r_i dr_i$, and $\rho_e(r_i, z_i, t)$ is net spin density along the z axis in the cylinder.

The microsphere is assumed to be right above the center of the cylinder, so that the magnetic field in the microsphere is approximately uniform in the transverse direction. Thus, the magnetic force produced by a cylinder

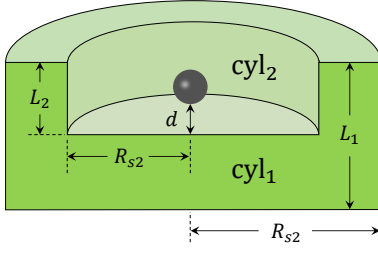


FIG. 7. The spin source consisting of a large cylinder (cylinder1) with a small cylinder (cylinder2) removed. R_{s1} and R_{s2} are radius of the two cylinders, and L_1 and L_2 are their heights, respectively. The gray ball represents the microsphere. d is the surface distance between the microsphere and the spin-source.

on this microsphere is

$$F_{s_{cy1}}(t) = \int_m dV \frac{\chi_m}{\mu_0} \left(B_{0z} \frac{\partial B_{szi}}{\partial z} + B_{szi} \frac{\partial B_{0z}}{\partial z} \right), \quad (C3)$$

where $\int_m dV$ is the integral over the microsphere. Therefore, the magnetic force produced by the spin-source on the microsphere is as follows:

$$F_s(t) = F_{s_{cy1}} - F_{s_{cy2}} \\ = \rho_e(t) \frac{\chi_m \mu_B}{2} \frac{\partial B_{0z}}{\partial z} \zeta_s(d, R), \quad (C4)$$

where $\zeta_s(d, R)$ is the effective volume for $F_s(t)$, reads:

$$\zeta_s(d, R) = \int_m dV \left(\frac{B_{0z}}{\frac{\partial B_{0z}}{\partial z}} \left(\frac{R_{s1}^2}{\sqrt{(R_{s1}^2 + z'^2)^3}} - \frac{R_{s1}^2}{\sqrt{(R_{s1}^2 + (z' + L_1)^2)^3}} - \frac{R_{s2}^2}{\sqrt{(R_{s2}^2 + z'^2)^3}} + \frac{R_{s2}^2}{\sqrt{(R_{s2}^2 + (z' + L_2)^2)^3}} \right) \right. \\ \left. + \left(\frac{z'}{\sqrt{R_{s1}^2 + z'^2}} - \frac{z' + L_1}{\sqrt{R_{s1}^2 + (z' + L_1)^2}} - \frac{z'}{\sqrt{R_{s2}^2 + (z' + L_2)^2}} + \frac{z' + L_2}{\sqrt{R_{s2}^2 + (z' + L_2)^2}} \right) \right). \quad (C5)$$

In the cylindrical coordinate system, we have $\int_m dV = \int_{-R}^R dz \int_0^{\sqrt{R^2 - z^2}} 2\pi r dr$, and $z' = z - L_2 - d - 3R$.

The geometry shape and the imperfections on fabrications are considered. The geometric parameters are optimized to make F_s as small as possible. Table II lists the optimized geometric parameters and their standard deviations according to the practical condition. Here we exaggerate the $\rho_e(t)$ to be ρ_{e0} . From the table, we can see that the value of optimized F_s is 4.2×10^{-22} N, while the total uncertainty of ΔF_s is $\Delta F_s = 5.03 \times 10^{-20}$ N. More generally, the variation of ΔF_s versus the standard deviations of geometric parameters is plotted in Fig. 8.

TABLE II. Structure parameters of the spin source plotted in FIG. 7 and their effects. The optimized geometrical parameters and their standard deviations are listed in the second column. After optimization, $\zeta_s = 10^{-23} \text{m}^3$ and $F_s = 4.2 \times 10^{-22} \text{N}$. $\Delta \zeta_s$ and ΔF_s due to parameter uncertainties are also listed. The total uncertainty of F_s is listed at bottom right corner, which is far greater than the value of F_s .

Parameter	Size(μm)	$\zeta_s(10^{-22} \text{m}^3)$	$F_s(10^{-21} \text{N})$
L_1	59.703 ± 0.003	-0.1 ∓ 5.0	-0.42 ∓ 18.2
L_2	48.674 ± 0.003	-0.1 ∓ 8.1	-0.42 ∓ 29.3
R_1	460.00 ± 0.003	-0.1 ∓ 6.4	-0.42 ∓ 23.4
R_2	440.93 ± 0.003	-0.1 ∓ 7.5	-0.42 ∓ 27.3
d	1.46 ± 0.001	-0.1 ∓ 1.1	-0.42 ∓ 4.29
R	3.2 ± 0.1	-0.1 ± 1.3	-0.42 ± 4.87
Total		-0.1 ± 13.8	-0.42 ± 50.3

The PSD of the spin-induced magnetic force reads:

$$S_{ff}^s(\omega) = \mathcal{F}(\langle F_s(t) | F_s(0) \rangle) \\ = \left(\frac{1}{2} \mu_B \chi_m \zeta_s(R, d) \frac{\partial B_{0z}}{\partial z} \right)^2 \mathcal{F}(\langle \rho_e(t) | \rho_e(0) \rangle) \\ = \left(\frac{1}{2} \mu_B \chi_m \zeta_s(R, d) \frac{\partial B_{0z}}{\partial z} \right)^2 \rho_{e0}^2 \tilde{G}(\omega) \\ = (F_s + \Delta F_s)^2 \tilde{G}(\omega) \\ \approx (\Delta F_s)^2 \tilde{G}(\omega) \quad (C6)$$

Appendix D: PSD OF SPIN-MASS FORCE

The spin-mass effective magnetic field generated by a polarized spin on an unpolarized nucleon is:

$$\mathbf{B}_{sp}(\mathbf{r}) = \frac{\hbar g_s^N g_p^e}{4\pi m_e \gamma} \left(\frac{1}{r\lambda} + \frac{1}{r^2} \right) e^{-r/\lambda} \mathbf{e}_r. \quad (D1)$$

The spin-mass effective magnetic field generated by the microsphere on a polarized spin is obtained by integrating the volume of the microsphere with Eq. (D1), i.e.,

$$\mathbf{B}_m = \int_m dV \rho_m \mathbf{B}_{sp}(\mathbf{r}) = \frac{\rho_m \hbar g_s^N g_p^e}{4\pi m_e \gamma} g(R, \ell) \mathbf{e}_\ell, \quad (D2)$$

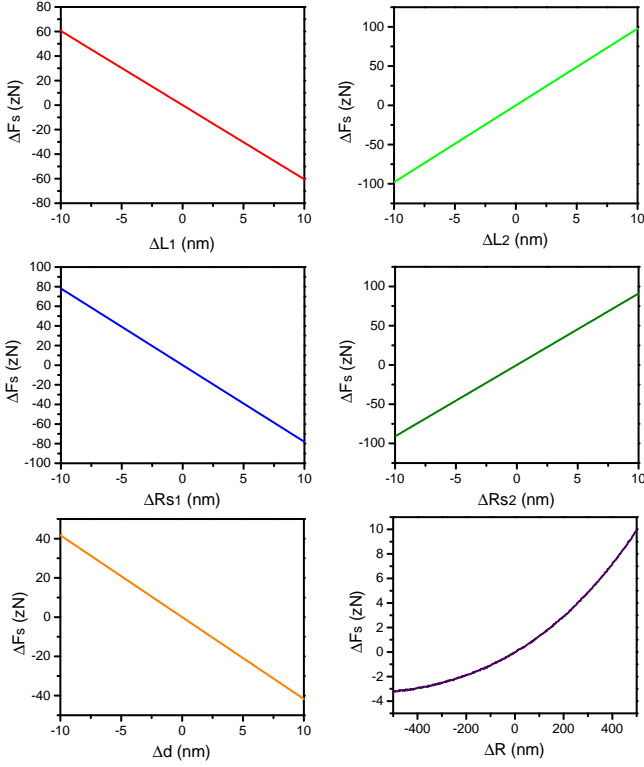


FIG. 8. Variation of ΔF_{s0} (standard deviation of F_{s0}) with ΔL_1 , ΔL_2 , ΔR_{s1} , ΔR_{s2} , ΔR , Δd calculated based on Eq. (C4) and Eq. (C5).

where

$$g(R, \ell) = 2\pi\lambda^2 \left((R - \lambda) e^{\frac{R}{\lambda}} + (R + \lambda) e^{-\frac{R}{\lambda}} \right) \left(\frac{1}{\lambda\ell} + \frac{1}{\ell^2} \right) e^{-\frac{\ell}{\lambda}}, \quad (\text{D3})$$

ρ_m is the nucleon density of microsphere, \mathbf{e}_ℓ and ℓ are the unit vector and distance between the microsphere and the spin, respectively. From Eq. (D2) and Eq. (D3), we can find that in the calculation of spin-mass effective magnetic field, the microsphere is completely equivalent to a center mass. Therefore, Eq. (D2) is equivalent to the effective magnetic field produced by the CM of the microsphere.

The spin-mass potential between the microsphere and the spin-source is obtained by integrating the volume of spin-source with Eq. (D2):

$$V_{sm}(t) = \int_{cy_1} dV \rho_e(r_1, z_1, t) \boldsymbol{\mu}_B \cdot \mathbf{B}_m - \int_{cy_2} dV \rho_e(r_2, z_2, t) \boldsymbol{\mu}_B \cdot \mathbf{B}_m,$$

and $\rho_e(r_i, z_i, t)$ represents the net electron spin density along the z axis in the spin-source.

Consequently, the spin-mass force between the micro-

sphere and the spin-source is

$$F_{sm}(t) = -\frac{\partial V_{sm}}{\partial z} = -\frac{\partial}{\partial z} \left(\int_{cy_1} dV \rho_e(r_1, z_1, t) \boldsymbol{\mu}_B \cdot \mathbf{B}_m - \int_{cy_2} dV \rho_e(r_2, z_2, t) \boldsymbol{\mu}_B \cdot \mathbf{B}_m \right),$$

where $\zeta_{sm}(R, d, \lambda)$ is the effective volume for $F_{sm}(t)$, reads:

$$\zeta_{sm}(R, d, \lambda) = (2\pi\lambda)^2 \left((R - \lambda) e^{-\frac{d}{\lambda}} + (R + \lambda) e^{-\frac{2R+d}{\lambda}} \right). \quad (\text{D4})$$

Accordingly, The PSD of spin-mass force reads:

$$\begin{aligned} S_{ff}^{sm}(\omega) &= \mathcal{F}(\langle F_s(t) | F_s(0) \rangle) \\ &= \left(\frac{\hbar^2 g_s^N g_p^e \rho_m}{8\pi m_m} \zeta_{sm}(R, d, \lambda) \right)^2 \mathcal{F}(\langle \rho_e(t) | \rho_e(0) \rangle) \\ &= \left(\frac{\hbar^2 g_s^N g_p^e \rho_m}{8\pi m_m} \zeta_{sm}(R, d, \lambda) \right)^2 \rho_{e_0}^2 \tilde{G}(\omega). \end{aligned} \quad (\text{D5})$$

Appendix E: CALCULATION OF $(g_s^N g_p^e)_{\text{limit}}$

To observe the spin-mass signal, $g_s^N g_p^e$ needs to be no less than

$$\begin{aligned} (g_s^N g_p^e)_{\text{limit}} &= \sqrt{\frac{S_{ff}^s(\omega_z)}{\tilde{G}(\omega_z)}} \frac{8\pi m_e}{\zeta_{sm} \hbar^2 \rho_m \rho_{e_0}} \\ &= \frac{\frac{\chi_m \mu_B}{2} \frac{\partial B_{0z}}{\partial z} \zeta_s(d, R)}{\frac{\hbar^2 \rho_m}{8\pi m_e} \zeta_{sm}(R, d, \gamma)}. \end{aligned}$$

For the worst situation, $(g_s^N g_p^e)_{\text{limit}}$ takes its upper bound:

$$\sup((g_s^N g_p^e)_{\text{limit}}) = \frac{\sup\left(\frac{\chi_m \mu_B}{2} \frac{\partial B_{0z}}{\partial z} \zeta_s(d, R)\right)}{\min\left(\frac{\hbar^2 \rho_m}{8\pi m_e} \zeta_{sm}(R, d, \gamma)\right)}, \quad (\text{E1})$$

where $\sup\left(\frac{\chi_m \mu_B}{2} \frac{\partial B_{0z}}{\partial z} \zeta_s(d, R)\right)$ means the upper bound of $\frac{\chi_m \mu_B}{2} \frac{\partial B_{0z}}{\partial z} \zeta_s(d, R)$, and $\min\left(\frac{\hbar^2 \rho_m}{8\pi m_e} \zeta_{sm}(R, d, \lambda)\right)$ is the minimum value of $\frac{\hbar^2 \rho_m}{8\pi m_e} \zeta_{sm}(R, d, \lambda)$. We take

$$\begin{aligned} &\sup\left(\frac{\chi_m \mu_B}{2} \frac{\partial B_{0z}}{\partial z} \zeta_s(d, R)\right) \\ &= \frac{\chi_m \mu_B}{2} \frac{\partial B_{0z}}{\partial z} (\zeta_s(d, R) + \Delta \zeta_s(d, R)) \\ &\approx \Delta F_s. \end{aligned} \quad (\text{E2})$$

and $\min\left(\frac{\hbar^2 \rho_m}{8\pi m_e} \zeta_{sm}(R, d, \lambda)\right)$ is numerically calculated with parameters R and d taken within the uncertainty ranges (see Table II). Combined with Eq. (E1) and Eq. (E2), the estimated $(g_s^N g_p^e)_{\text{limit}}$ in the worst situation is shown in red in Fig. 3 in the main text.

-
- [1] S. Weinberg, *Phys. Rev. Lett.* **40**, 223 (1978).
 - [2] F. Wilczek, *Phys. Rev. Lett.* **40**, 279 (1978).
 - [3] R. D. Peccei and H. R. Quinn, *Phys. Rev. Lett.* **38**, 1440 (1977).
 - [4] R. D. Peccei and H. R. Quinn, *Phys. Rev. D* **16**, 1791 (1977).
 - [5] S. J. Asztalos, L. J. Rosenberg, K. van Bibber, P. Sikivie, and K. Zioutas, *Annual Review of Nuclear and Particle Science* **56**, 293 (2006).
 - [6] A. Arvanitaki, S. Dimopoulos, S. Dubovsky, N. Kaloper, and J. March-Russell, *Phys. Rev. D* **81**, 123530 (2010).
 - [7] M. Cicoli, M. D. Goodsell, and A. Ringwald, *Journal of High Energy Physics* **2012**, 146 (2012).
 - [8] A. A. Anselm and N. G. Uraltsev, *Physics Letters B* **114**, 39 (1982).
 - [9] L. Krauss, J. Moody, F. Wilczek, and D. E. Morris, *Phys. Rev. Lett.* **55**, 1797 (1985).
 - [10] J. Redondo and A. Ringwald, *Contemporary Physics* **52**, 211 (2011).
 - [11] R. Ballou, G. Deferne, M. Finger, M. Finger, L. Flekova, J. Hosek, S. Kunc, K. Macuchova, K. A. Meissner, P. Pugnat, M. Schott, A. Siemko, M. Slunecka, M. Sulc, C. Weinsheimer, and J. Zicha (OSQAR Collaboration), *Phys. Rev. D* **92**, 092002 (2015).
 - [12] P. Sikivie, *Phys. Rev. Lett.* **51**, 1415 (1983).
 - [13] C. Collaboration, *Nature Physics* **13**, 584 (2017).
 - [14] G. Raffelt and L. Stodolsky, *Phys. Rev. D* **37**, 1237 (1988).
 - [15] M. Fouché, R. Battesti, and C. Rizzo, *Phys. Rev. D* **93**, 093020 (2016).
 - [16] E. G. Adelberger, B. R. Heckel, S. Hoedl, C. D. Hoyle, D. J. Kapner, and A. Upadhye, *Phys. Rev. Lett.* **98**, 131104 (2007).
 - [17] D. J. Wineland, J. J. Bollinger, D. J. Heinzen, W. M. Itano, and M. G. Raizen, *Phys. Rev. Lett.* **67**, 1735 (1991).
 - [18] B. J. Venema, P. K. Majumder, S. K. Lamoreaux, B. R. Heckel, and E. N. Fortson, *Phys. Rev. Lett.* **68**, 135 (1992).
 - [19] A. N. Youdin, D. Krause, Jr., K. Jagannathan, L. R. Hunter, and S. K. Lamoreaux, *Phys. Rev. Lett.* **77**, 2170 (1996).
 - [20] W.-T. Ni, S.-s. Pan, H.-C. Yeh, L.-S. Hou, and J. Wan, *Phys. Rev. Lett.* **82**, 2439 (1999).
 - [21] K. Tullney, F. Allmendinger, M. Burghoff, W. Heil, S. Karpuk, W. Kilian, S. Knappe-Grüneberg, W. Müller, U. Schmidt, A. Schnabel, F. Seifert, Y. Sobolev, and L. Trahms, *Phys. Rev. Lett.* **111**, 100801 (2013).
 - [22] M. Bulatowicz, R. Griffith, M. Larsen, J. Mirijanian, C. B. Fu, E. Smith, W. M. Snow, H. Yan, and T. G. Walker, *Phys. Rev. Lett.* **111**, 102001 (2013).
 - [23] N. Crescini, C. Braggio, G. Carugno, P. Falferi, A. Ortolan, and G. Ruoso, *Physics Letters B* **773**, 677 (2017).
 - [24] G. Vasilakis, J. M. Brown, T. W. Kornack, and M. V. Romalis, *Phys. Rev. Lett.* **103**, 261801 (2009).
 - [25] W. A. Terrano, E. G. Adelberger, J. G. Lee, and B. R. Heckel, *Phys. Rev. Lett.* **115**, 201801 (2015).
 - [26] J. E. Moody and F. Wilczek, *Phys. Rev. D* **30**, 130 (1984).
 - [27] G. D. Hammond, C. C. Speake, C. Trenkel, and A. P. Patón, *Phys. Rev. Lett.* **98**, 081101 (2007).
 - [28] A. Arvanitaki and A. A. Geraci, *Phys. Rev. Lett.* **113**, 161801 (2014).
 - [29] M. S. Turner, *Physics Reports* **197**, 67 (1990).
 - [30] M. P. Ledbetter, M. V. Romalis, and D. F. J. Kimball, *Phys. Rev. Lett.* **110**, 040402 (2013).
 - [31] J. Gieseler, L. Novotny, and R. Quidant, *Nature Physics* **9**, 806 (2013).
 - [32] G. Ranjit, M. Cunningham, K. Casey, and A. A. Geraci, *Phys. Rev. A* **93**, 053801 (2016).
 - [33] B. R. Slezak, C. W. Lewandowski, J.-F. Hsu, and B. D’Urso, *New Journal of Physics* **20**, 063028 (2018).
 - [34] J. Ahn, Z. Xu, J. Bang, Y.-H. Deng, T. M. Hoang, Q. Han, R.-M. Ma, and T. Li, *Phys. Rev. Lett.* **121**, 033603 (2018).
 - [35] F. Ricci, M. T. Cuairan, G. P. Conangla, A. W. Schell, and R. Quidant, *Nano Letters* **19**, 6711 (2019).
 - [36] F. Monteiro, W. Li, G. Afek, C.-I. Li, M. Mossman, and D. C. Moore, *Phys. Rev. A* **101**, 053835 (2020).
 - [37] D. C. Moore and A. A. Geraci, *arXiv e-prints*, [arXiv:2008.13197](https://arxiv.org/abs/2008.13197) (2020).
 - [38] A. A. Geraci, S. B. Papp, and J. Kitching, *Phys. Rev. Lett.* **105**, 101101 (2010).
 - [39] D. E. Chang, C. A. Regal, S. B. Papp, D. J. Wilson, J. Ye, O. Painter, H. J. Kimble, and P. Zoller, *Proceedings of the National Academy of Sciences* **107**, 1005 (2010).
 - [40] D. S. Ether, L. B. Pires, S. Umrath, D. Martinez, Y. Ayala, B. Pontes, G. R. de S. Araújo, S. Frases, G. L. Ingold, F. S. S. Rosa, N. B. Viana, H. M. Nussenzeveig, and P. A. Maia Neto, *Europhysics Letters* **112**, 44001 (2015).
 - [41] A. D. Rider, D. C. Moore, C. P. Blakemore, M. Louis, M. Lu, and G. Gratta, *Phys. Rev. Lett.* **117**, 101101 (2016).
 - [42] E. Hebestreit, M. Frimmer, R. Reimann, and L. Novotny, *Phys. Rev. Lett.* **121**, 063602 (2018).
 - [43] G. Winstone, R. Bennett, M. Rademacher, M. Rashid, S. Buhmann, and H. Ulbricht, *Phys. Rev. A* **98**, 053831 (2018).
 - [44] Y. Leng, R. Li, X. Kong, H. Xie, D. Zheng, P. Yin, F. Xiong, T. Wu, C. Kui Duan, Y. Du, Z. q. Yin, P. Huang, and J. Du, *arXiv e-prints*, [arXiv:2008.07940](https://arxiv.org/abs/2008.07940) (2020).
 - [45] A. A. Clerk, M. H. Devoret, S. M. Girvin, F. Marquardt, and R. J. Schoelkopf, *Rev. Mod. Phys.* **82**, 1155 (2010).
 - [46] D. Zheng, Y. Leng, X. Kong, R. Li, Z. Wang, X. Luo, J. Zhao, C.-K. Duan, P. Huang, J. Du, M. Carlesso, and A. Bassi, *Phys. Rev. Research* **2**, 013057 (2020).
 - [47] F. Tebbenjohanns, M. Frimmer, A. Militaru, V. Jain, and L. Novotny, *Phys. Rev. Lett.* **122**, 223601 (2019).
 - [48] E. C. Reynhardt, G. L. High, and J. A. van Wyk, *J. Chem. Phys.* **109**, 8471 (1998).
 - [49] S. Takahashi, R. Hanson, J. van Tol, M. S. Sherwin, and D. D. Awschalom, *Phys. Rev. Lett.* **101**, 047601 (2008).
 - [50] X. Rong, M. Wang, J. Geng, X. Qin, M. Guo, M. Jiao, Y. Xie, P. Wang, P. Huang, F. Shi, Y.-F. Cai, C. Zou, and J. Du, *Nature Communications* **9**, 739 (2018).
 - [51] S. A. Hoedl, F. Fleischer, E. G. Adelberger, and B. R. Heckel, *Phys. Rev. Lett.* **106**, 041801 (2011).
 - [52] B. R. Heckel, E. G. Adelberger, C. E. Cramer, T. S. Cook, S. Schlamminger, and U. Schmidt, *Phys. Rev. D* **78**, 092006 (2008).
 - [53] J. Lee, A. Almasi, and M. Romalis, *Phys. Rev. Lett.*

- [120](#), [161801](#) (2018).
- [54] G. L. Klimchitskaya and V. M. Mostepanenko, [Proceedings of Peter the Great St. Petersburg Polytechnic University](#), [41](#) (2015).
- [55] G. L. Klimchitskaya, U. Mohideen, and V. M. Mostepanenko, [Phys. Rev. A](#) **61**, [062107](#) (2000).
- [56] M. Bordag, U. Mohideen, and V. M. Mostepanenko, [Physics Reports](#) **353**, [1](#) (2001).
- [57] R. S. Decca, D. López, E. Fischbach, and D. E. Krause, [Phys. Rev. Lett.](#) **91**, [050402](#) (2003).